Mon. Not. R. Astron. Soc. **000**, 000–000 (0000) Printed 15 January 2013 (MN LATEX style file v2.2)

Orbital and Evolutionary Constraints on the Planet Hosting Binary GJ 86 from the *Hubble Space Telescope*

J. Farihi[1,2⋆†], Howard E. Bond[3,4‡], P. Dufour[5], N. Haghighipour[6], G. H. Schaefer[7], J. B. Holberg[8] M. A. Barstow[2], M. R. Burleigh[2]

[1] *Institute of Astronomy, University of Cambridge, Cambridge CB3 0HA*
[2] *Department of Physics & Astronomy, University of Leicester, Leicester LE1 7RH*
[3] *Space Telescope Science Institute, Baltimore, MD 21218, USA*
[4] *Department of Astronomy & Astrophysics, Pennsylvania State University, University Park, PA 16802, USA*
[5] *Département de Physique, Université de Montréal, Montréal, QC H3C 3J7, Canada*
[6] *Institute for Astronomy, University of Hawaii-Manoa, Honolulu, HI 96822, USA*
[7] *CHARA Array of Georgia State University, Mount Wilson Observatory, CA 91023, USA*
[8] *Lunar and Planetary Laboratory, University of Arizona, Tucson AZ 85721, USA*

ABSTRACT

This paper presents new observations of the planet-hosting, visual binary GJ 86 (HR 637) using the *Hubble Space Telescope*. Ultraviolet and optical imaging with WFC3 confirms the stellar companion is a degenerate star and indicates the binary semimajor axis is larger than previous estimates, with $a \gtrsim 28$ AU. Optical STIS spectroscopy of the secondary reveals a helium-rich white dwarf with C_2 absorption bands and $T_{\rm eff} = 8180$ K, thus making the binary system rather similar to Procyon. Based on the 10.8 pc distance, the companion has $0.59\,M_{\odot}$ and descended from a main-sequence A star of $1.9\,M_{\odot}$ with an original orbital separation $a \gtrsim 14$ AU. If the giant planet is coplanar with the binary, the mass of GJ 86Ab is between 4.4 and 4.7 $M_{\rm Jup}$.

The similarity of GJ 86 and Procyon prompted a re-analysis of the white dwarf in the latter system, with the tentative conclusion that Procyon hosts a planetesimal population. The periastron distance in Procyon is 20% smaller than in α Cen AB, but the metal-enriched atmosphere of Procyon B indicates that the planet formation process minimally attained 25 km bodies, if not small planets as in α Cen.

Key words: binaries: visual— stars: individual (GJ 86A, GJ 86B)— planetary systems— white dwarfs

1 INTRODUCTION

About 20% of known extrasolar planets orbit one component of a stellar binary (Raghavan et al. 2006; Haghighipour 2006). Both observation and theory indicate that the majority of these planets in binaries are similar to those orbiting single stars, owing to the wide ($a > 100$ AU) stellar separations (Desidera & Barbieri 2007; Haghighipour 2006). However, there are a growing number of systems which present a major challenge to planet-formation modelers, because their *giant* planets orbit one component within closer binary systems. In order of discovery, these planetary systems are GJ 86 (HR 637, HD 13445) (Queloz et al. 2000), γ Cephei (Hatzes et al. 2003), HD 41004 (Zucker et al. 2004), HD 196885 (Correia et al. 2008), and HD 17605 (Muterspaugh et al. 2010). All five of these binaries are thought to have $a \lesssim 30$ AU and a giant planet orbiting the primary star. However, only in GJ 86 is the stellar secondary a white dwarf rather than a second main-sequence star, and the Jovian planet thus orbits the originally *less* massive component. Furthermore, the initial binary separation was smaller, making GJ 86 a challenging environment in which to form planets.

Our view of planet formation in binaries has changed significantly in the past 17 years. Simulations of binary stars with $a < 40$ AU failed to retain sufficient circumstellar material to form planets around one star, and thus precluded planet birth by either the core accretion or disk-instability mechanisms (Nelson 2000; Artymowicz & Lubow

⋆ E-mail: jfarihi@ast.cam.ac.uk
† STFC Ernest Rutherford Fellow
‡ Current address: 9615 Labrador Lane, Cockeysville, MD 21030, USA

Table 1. *HST* Cycle 19 Observations of GJ 86B

Instrument	UT Date	Filter/Grating	Exposures (s)
WFC3 UVIS	2012 Mar 31	F225W	1.0×16
		F225W	20.0×4
		F275W	10.0×4
		F336W	5.0×4
		F390W	4.0×4
		F438W	4.0×4
		F555W	2.0×4
		F625W	2.0×4
		F814W	30.0×4
STIS CCD	2012 May 29	G430L	100.0×3
		G430M	600.0×4
		G750M	400.0×3

Table 2. Flux Densities & Effective Wavelengths for GJ 86B[a]

Filter	$\lambda_{\rm eff}^{b}$ (Å)	$F_\lambda \,/\, 10^{-14}$ (erg s^{-1} cm^{-2} Å^{-1})	$F_\nu \,/\, 10^{-26}$ (erg s^{-1} cm^{-2} Hz^{-1})
F225W	2385	3.49	6.62
F275W	2722	4.04	9.99
F336W	3355	3.93	14.76
F390W	3908	3.40	17.34
F438W	4315	3.02	18.75
F555W	5237	2.18	19.91
F625W	6183	1.56	19.87
F814W	7899	0.80	16.74

[a] The flux of GJ 86A was measured to be 31.4 mJy in F225W.
[b] Effective wavelengths were derived by convolving the adopted stellar model in F_λ with the WFC3 filter transmission curves.

1994; see Prato & Weinberger 2010 for a detailed review). Yet observers have imaged favorable planet-forming environments around the components of close binary stars, implying planet formation in these systems may be as common as around single stars (Akeson et al. 1998; Mathieu 1994). For example, the two well-separated disks in the binary system L1551 (Rodriguez et al. 1998) indicate that, despite disk truncation, it is still possible for both components to retain a significant amount of their original circumstellar material ($0.03 - 0.06\,M_\odot$) in disks with considerable radii ($r \approx 10$ AU). These disk masses are comparable to the minimum-mass model of the primordial Solar nebula (Hayashi 1981; Weidenschilling 1977) suggesting that planet formation in these environments may proceed as in disks around single stars.

The Jovian planet[1] orbiting GJ 86A (K0 V) was discovered via precision radial-velocity monitoring (Queloz et al. 2000), revealing a 15.8 d orbit (0.11 AU separation) with $m \sin i = 4\,M_{\rm Jup}$. At the time of discovery, an additional long-term radial velocity drift was reported, suggesting the presence of a more distant, unseen stellar companion. Subsequently, the distant companion was directly detected at a projected separation of $1\farcs7$, but 9 mag fainter than the primary in the K band (Els et al. 2001). The companion, GJ 86B, was later imaged by Mugrauer & Neuhäuser (2005) and Lagrange et al. (2006) whose data clearly reveal orbital motion; between 2000 and 2005 the angular separation of the pair changed by $0\farcs25$ and the position angle changed by 17°. GJ 86B cannot be a low-mass star or brown dwarf: a substellar mass cannot be reconciled with the observed radial-velocity drift of GJ 86A, and follow-up methane-band photometry showed GJ 86B to have a near-IR color index near zero. Moreover, K-band spectroscopy of GJ 86B reveals an essentially Rayleigh-Jeans continuum source. Thus, GJ 86B can only be a white dwarf (Lagrange et al. 2006; Mugrauer & Neuhäuser 2005).

In order to ideally constrain the formation and evolution of the giant planet orbiting GJ 86A, it is necessary to obtain the orbit and component masses of the binary system. The 3300:1 contrast ratio between components in the infrared makes this difficult but possible with adaptive optics, yet white dwarfs do not exhibit spectral features in this wavelength region. Thus an optical study of GJ 86B is necessary and a *Hubble Space Telescope (HST)* program was initiated to achieve this goal. In §2 are described the imaging and spectroscopic observations, while §3 describes the atmospheric modeling, derivation of current (and progenitor) stellar parameters and binary orbit constraints. New static limits on the GJ 86 planetary system are calculated based on the *HST* observations and possible similarities with the Procyon system are discussed in §4.

[1] The planet is often referred to incorrectly as GJ 86b, while the correct designation is GJ 86Ab

2 OBSERVATIONS & DATA REDUCTION

Due to orbital motion observed between 2000 and 2005 (Lagrange et al. 2006; Mugrauer & Neuhäuser 2005), it was expected that precise spatial offsets might be necessary for proper placement of the faint companion within the spectroscopic aperture. Thus, WFC3 imaging was executed for both photometric and astrometric purposes, prior to STIS spectroscopy.

2.1 WFC3 Imaging

GJ 86 was imaged on 2012 March 31 using the Wide Field Camera 3 (WFC3) in the UVIS channel with a 512×512 (UVIS2-C512C-SUB) subarray. The imaging sequence took place over a single orbit and began with a series of 1 s exposures in the F225W filter. In this short exposure time, the flux from the $V = 6.2$ mag, $T_{\rm eff} \approx 5200$ K primary was expected to leave an unsaturated, linear response on the CCD. This sequence employed the default UVIS dither pattern with four points in a parallelogram, and was repeated four times for a total of 16 exposures. Both primary and secondary star were well-detected in this first set of exposures, and in the linear response regime with high signal-to-noise (S/N) > 500. This set of images was used to robustly measure the separation of the binary, where the secondary star was found at offset:

$$\alpha = 2\farcs351(2) \quad \theta = 88\fdg96(4)\ \text{(J2000)} \quad \text{Date: 2012.2468}$$

Immediately following the short exposure sequence, a single dither pattern of four deeper exposures was executed in each of eight filters (see Table 1 and Figure 1). At the

Figure 1. Images of GJ 86 in the eight specified ultraviolet and optical filters using WFC3 UVIS. The images are oriented so that upward is 17.°60 east of north, and each frame is 8″ on a side. The bottom-right image is a composite RGB frame using the F225W (blue), F275W (green), and F336W (red) filters. A series of short exposures at F225W were obtained with an unsaturated primary, and these data were used for the relative astrometry of the pair.

phase II design stage, the brightness of the companion was poorly constrained and the longer exposures were to insure high S/N photometry (up to the limit imposed by the PSF wings of the primary) at all wavelengths. Fortunately, even without stray light correction, the dither-combined image sets yielded S/N > 500 for GJ 86B shortward of 5500 Å, and S/N > 200 beyond. Thus, the relatively faint companion was mostly unaffected by the primary.

Photometry was performed on multi-drizzled images produced by the STScI software and data pipeline OPUS 2012.1 and CALWF3 2.6.2. The flux of GJ 86B was measured in an $r = 7$ pixel aperture radius and corrected using the encircled energy data available in the WFC3 Instrument Handbook version 3.0 (Dressel et al. 2010). The aperture corrections were derived by interpolating the tabular values at the effective wavelength of the best fitting atmospheric model (see §3) in each bandpass, and the process was iterated until there were no significant changes in the photometry or stellar model parameters; in practice this occurred after a single repetition. The background flux of GJ 86A was subtracted by examining points opposite, in x and y on the subarray, from the bright primary. This ambient light cor-

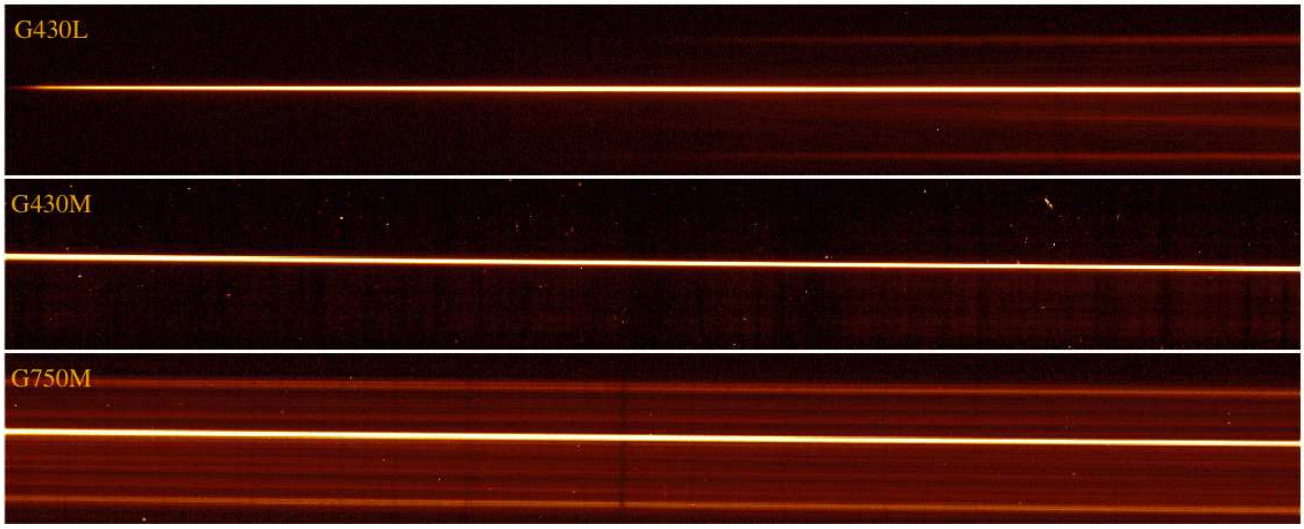

Figure 2. Combined-frame STIS CCD spectral images of GJ 86B taken in three gratings, with wavelength increasing to the right. The ambient light of the primary is relatively mild, even in red light. Despite rejection routines that drastically reduced the number of cosmic rays, hot and cold pixels present in the single exposures, some artifacts remain in the combined 2D images, especially at the shortest wavelength setting.

rection resulted in flux measurement changes less than 1.2% for the five filters below 5000 Å, but rose to around 4% for the three longer wavelength filters. The measured fluxes for GJ 86B are listed in Table 2.

2.2 STIS Spectroscopy

Observations with the Space Telescope Imaging Spectrograph (STIS) were executed on 2012 May 29, beginning with an acquisition sequence of GJ 86A, followed by an offset and acquisition/peak-up of GJ 86B based on the WFC3 astrometry. Examination of the acquisition and peak-up images shows they were successful. Spectroscopy was performed with the G430L, G430M, and G750M gratings as detailed in Table 1, using default STIS dither patterns along the slit, and achieving average resolutions of 6.8, 0.7, and 1.4 Å, respectively.

The individual spectral images were first shifted onto a common frame as indicated by the image header astrometry and using integer pixel shifts. Next, the shifted images were combined into a single 2D frame using MSCOMBINE in the IRAF STSDAS software package. Prior to this step, the spectral images contained a significant number of bad pixels and cosmic rays, especially in the G430M observations. Rejection of these unwanted pixels was performed using CCDCLIP at 4σ, although this could not completely remove the accumulated artifacts.

Figure 2 shows the final, combined spectral images for each of the grating settings. Although stray light from the primary is apparent in all the images, and most readily seen in the red, the signal from GJ 86B was essentially unaffected. The contrast between the peak signals from the science target and the primary diffraction spikes was 17:1 at the lowest in the G750M observations, and at least twice as high in the region of the science spectrum.

Lastly, 1D spectra were extracted using X1D, and appropriate sky subtraction to correct for the relatively mild background. The flux-calibrated and normalized STIS spectra are displayed in Figures 3 and 4. The S/N per pixel was determined from continuum regions within each of the spectra to be close to 85, 88, and 53 in the G430L, G430M, and G750M gratings respectively.

3 STELLAR & BINARY PARAMETERS

The upper spectrum shown in Figure 4 displays the distinctive and broad C_2 Swan bands, indicating that GJ 86B has a DQ spectral classification. This class of white dwarfs is characterized by helium-dominated atmospheres with trace carbon, likely dredged from the core (Pelletier et al. 1986). Neither Ca II K nor Hα were detected in the relatively deep and higher resolution G430M and G750M spectra. Following convention the star has the white dwarf designation WD 0208−510 (McCook & Sion 1999).

3.1 Atmospheric Modeling

Stellar parameters for GJ 86B were derived in two ways, using model atmosphere grids appropriate for DQ white dwarfs (see Dufour et al. 2005 for details on the models and fitting techniques). First, the effective temperature and solid angle were estimated from fitting the broad baseline WFC3 photometry. These parameters were then combined with the Hipparcos parallax of 92.74 mas (van Leeuwen 2007; Perryman et al. 1997) to determine the stellar radius, which was then converted into mass using theoretical mass-radius relationships (Fontaine et al. 2001). However, the shape of the energy distribution – and thus the derived effective temperature – is slightly sensitive to the amount of photospheric carbon. Model fits to the C_2 Swan bands in the G430L STIS spectrum were used to measure the carbon abundance, with $T_{\rm eff}$ and $\log g$ fixed at the values obtained from the WFC3 photometry. The effective temperature and solid angle were re-derived using C/He fixed to the spectroscopic

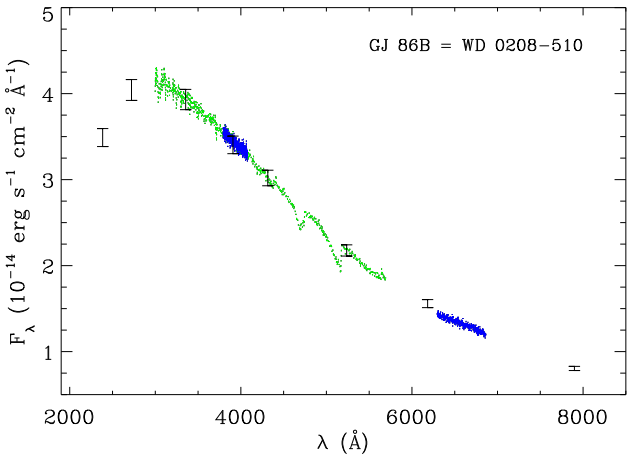

Figure 3. Flux-calibrated WFC3 photometry and STIS spectra of GJ 86B for each of the configurations specified in Table 1. Figure 4 plots the spectra in greater detail.

Table 3. Current & Progenitor Stellar Parameters for GJ 86AB

GJ 86B / WD 0208−510	
White Dwarf Remnant:	
SpT	DQ6
$V_{\rm eff}$ (mag)	13.2
$T_{\rm eff}$ (K)	8180 ± 120
log g (cm s^{-2})	8.02 ± 0.02
Mass ($M_\odot$)	0.59 ± 0.01
Radius ($R_\odot$)	0.01245 ± 0.0015
Cooling Age (Gyr)	1.25 ± 0.05
log (C/He)	-4.8 ± 0.2
log (H/He)	< -4.3
log (Ca/He)	< -11.8
Main-Sequence Progenitor:	
SpT	A5 V
Mass ($M_\odot$)	1.9 ± 0.1
Lifetime (Gyr)	1.4 ± 0.2
GJ 86A / HR 637 / HD 13445	
SpT	K0 V
V (mag)	6.1
$T_{\rm eff}$ (K)	5200
Mass ($M_\odot$)	0.80
Age (Gyr)	2.5

Note. Parameters listed for GJ 86A are values representative of those found in the literature (Ghezzi et al. 2010; van Belle & von Braun 2009; Mamajek & Hillenbrand 2008; Valenti & Fischer 2005; Saffe et al. 2005; Ribas et al. 2003; Flynn & Morell 1997).

value. This procedure was iterated until all parameters converged, with a good fit obtained at $T_{\rm eff} = 8420 \pm 90$ K, log (C/He) $- 4.58 \pm 0.15$.

Second, because the STIS data are flux-calibrated with a high degree of confidence, the effective temperature and carbon abundance can be simultaneously obtained from the G430L spectrum alone, yielding $T_{\rm eff} = 8145 \pm 180$ K, log (C/He) $= -4.82 \pm 0.15$. The difference in resulting model

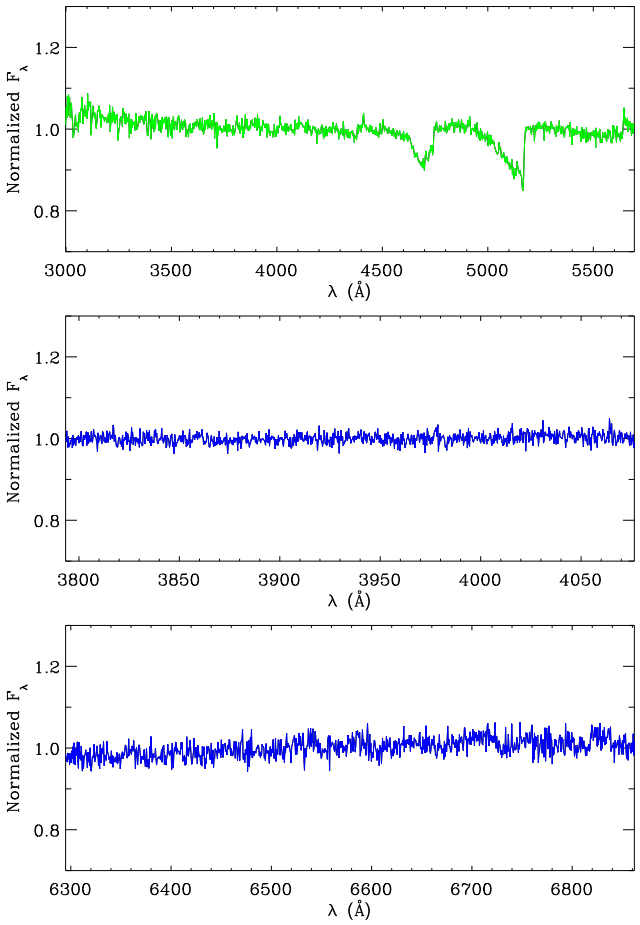

Figure 4. From top to bottom are normalized STIS spectra of GJ 86B obtained with the G430L, G430M, and G750M gratings. The only detected spectral features are the C_2 Swan bands. Upper limits on calcium and hydrogen were derived from the Ca II K and Hα regions (Table 3).

parameters is significant and most likely caused by the two shortest wavelength fluxes. Indeed, the F225W and F275W bandpasses span a region influenced by at least one strong C I line which models tend to over-predict (in the core or wings). An example of this was observed by Provencal et al. (2002) in the STIS ultraviolet spectrum of Procyon B, where the strength of the 2478 Åline is much weaker (by nearly a factor of 30 in C/He) than predicted by models. The model shortcomings are understood to be a consequence of the high density environments in cool helium-rich white dwarf photospheres; the classical Van der Waal broadening treatment within the impact approximation, traditionally used in DQ model atmospheres, is not appropriate for these lines (Koester et al. 1982).

If one ignores the two ultraviolet fluxes affected by these strong C I lines, and uses the remaining six WFC3 photometric data points, then $T_{\rm eff} = 8210 \pm 180$ K, log (C/He) $= -4.76 \pm 0.15$ is obtained, in agreement with the parameters from fitting the spectrum alone. For all stellar and evolutionary parameters, the weighted average of the photometric (ignoring F225W and F275W) and spectroscopic effective temperatures, and the non-weighted average of the carbon abundances are thus adopted and listed in Table 3

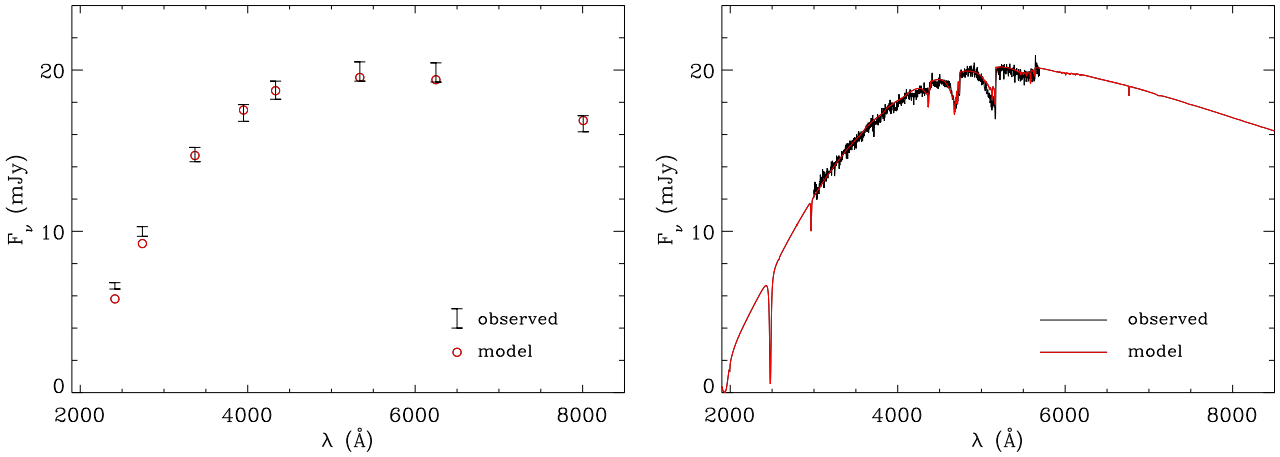

Figure 5. Comparison between the observed and modeled stellar fluxes. In the left-hand panel, the model fluxes agree well with the WFC3 photometry in all bandpasses except F225W and F275W (see §3.1). In the right-hand panel the model spectrum reproduces both the optical continuum and C_2 bands in the STIS G430L data, but indicates a strong C I 2478 Å feature that under-predicts the stellar flux in the two ultraviolet filters. All spectral features are due to atomic or molecular carbon.

($T_{\rm eff} = 8180 \pm 120$ K and $\log({\rm C/He}) = -4.8 \pm 0.2$). Upper limit hydrogen and calcium abundances were also derived and are listed in Table 3, while Figure 5 shows the best fitting model compared to the photometry and G430L spectrum. All the derived stellar parameters are listed in Table 3.

3.2 Current Binary Orbit

The epoch 2012.2 WFC3 imaging provides a new point along the binary orbit of GJ 86, and is shown in Figure 6 together with previous astrometric measurements (Lagrange et al. 2006; Els et al. 2001). Unfortunately, one quarter of the full orbit has not yet been observed, and hence the orbital parameters can only be loosely constrained. For all orbital calculations, $M_A = 0.8\,M_\odot$ and $M_B = 0.6\,M_\odot$ are adopted for simplicity; the actual component masses are not better constrained at present.

Using the new astrometric datum, a statistical analysis of orbits that fit the observations was performed. A Monte Carlo simulation of 10 000 orbital solutions was created with periods from 20 to 500 yr, eccentricities from 0.00 to 0.99, and with time of periastron passage from 1800 to 2200. From these solutions, the 100 orbits with the best χ^2 values, and with total masses within the limited range $M_{tot} = 1.4 \pm 0.1\,M_\odot$ were selected. These orbits are plotted in Figure 6, and the resulting range in orbital parameters is listed in Table 4. As can be seen, only the system inclination is significantly constrained at present. The solutions with low eccentricities tend to have relatively short orbital periods, whereas the longer period solutions require high eccentricities. Notably, the orbital solution with the shortest period yields a semimajor axis $a = 27.8$ AU with eccentricity $e = 0.10$, and is significantly larger than the representative solution with $a = 18.4$ AU adopted by Lagrange et al. (2006).

4 BINARY & PLANETARY EVOLUTION

4.1 Total System Age

The white dwarf cooling age places a firm lower limit of 1.3 Gyr on the lifetime of the system (Fontaine et al. 2001). For the total age, one must add the hydrogen-burning lifetime of the progenitor, which should be in the range $1.2 - 1.6$ Gyr for stars of mass $1.8 - 2.0\,M_\odot$. Thus, the evolved companion suggests a total system age of 2.65 ± 0.25 Gyr. Age estimates for the primary include $2.0 - 2.9$ Gyr (Saffe et al. 2005) and 2.4 Gyr (Mamajek & Hillenbrand 2008) based on activity-age relations, and these broadly agree with that derived for the secondary. Mamajek & Hillenbrand (2008) prefers an age of 3.7 Gyr based on activity-rotation-age metrics, but this value is significantly older than expected for the total lifetime of the white dwarf and its progenitor.

4.2 The Main-Sequence Progenitor System

To constrain formation scenarios for the giant planet orbiting GJ 86A, the binary orbit and component masses when both stars were on the main sequence is needed. Using initial-to-final mass relations with some empirical constraints at the low-mass end of progenitor and remnant masses (Williams et al. 2009; Kalirai et al. 2008), GJ 86B likely descended from a main-sequence, A-type star with a mass near $1.9\,M_\odot$. With both stars on the main sequence, the semimajor axis of the binary was smaller by a factor (Jeans 1924)

$$\frac{a_0}{a} = \frac{M_B + M_A}{M_{B_0} + M_A} \qquad (1)$$

This ratio is not very sensitive to the range of allowed masses, and yields $a_0 = 0.52a$ for $M_A = 0.80\,M_\odot$, $M_B = 0.59\,M_\odot$, $M_{B_0} = 1.86\,M_\odot$. A canonical mass value has been assumed for the primary, but is consistent with isochrones and various literature estimates (van Belle & von Braun 2009; Valenti & Fischer 2005; Ribas et al. 2003; Flynn & Morell 1997). From the

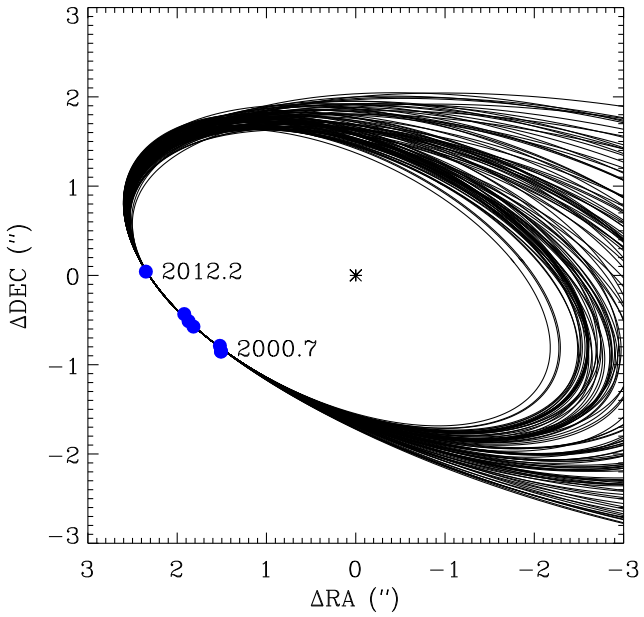

Figure 6. The blue data points are the astrometric offsets determined here using WFC3 (leftmost point), together with those reported by Lagrange et al. (2006) and Els et al. (2001). An initial sample of 10 000 orbital solutions were generated through a Monte Carlo search, and overplotted in black are the 100 orbits with the best χ^2 values, within the restricted mass range $M_{tot} = 1.4 \pm 0.1\,M_{\odot}$.

current binary orbit simulations, a lower limit on the initial semimajor axis is obtained $a_0 \geqslant 14.5$ AU. Even at this lower limit, the 0.11 AU planetary orbit of GJ 86Ab is stable for binary eccentricities $e < 0.9$ (Holman & Wiegert 1999; Rabl & Dvorak 1988).

4.3 Planetesimals in GJ 86

Although the class of detached binary stars with a white dwarf and a main-sequence component of spectral type K or earlier are referred to as Sirius-type binaries (Holberg et al. 2008), GJ 86 is also notably *Procyon-like*. Table 5 lists the atmospheric and stellar parameters for these two white dwarf companion systems, demonstrating their broad similarities.

Because GJ 86 is known to host a planetary system, with at least one giant planet orbiting the primary, it may also support a planetesimal population. These surviving minor bodies could be gravitationally perturbed into close encounters with the white dwarf, where they would be tidally shredded and eventually accreted, polluting the atmosphere with heavy elements (Jura 2003), as observed at nearly 30 single white dwarfs (Gänsicke et al. 2012; Farihi et al. 2012; Kilic et al. 2012; Debes et al. 2012). In a binary such as GJ 86, stable planetesimal belts can persist as circumstellar rings at either star, or a circumbinary disk.

One region that remains stable over both the current and former binary configurations and $e < 0.1$ is within roughly 3 AU of the K star primary. Stable circumstellar regions for the white dwarf are complicated by competing processes: while the region within 2 AU will be depleted of small bodies by direct engulfment and tides during the giant phases (Mustill & Villaver 2012), surviving objects will have their orbit expanded due to mass loss, by a factor of $M_{B_0}/M_B \approx 3.2$. However, the critical radius for stability also increases due to mass loss, but by a factor smaller than $(M_B + M_A)/(M_{B_0} + M_A) \approx 1.9$, and therefore a narrow range of stable, planetesimal orbits are possible for the white dwarf if $a \gtrsim 30$ AU currently. It is worth noting that these calculations are purely static, and thus ignore the dynamic effects of mass loss which may have significant impact on stable orbits (Veras & Tout 2012; Veras et al. 2011). Circumbinary orbits beyond 80 AU are also stable in the current and former binary configurations for $a \approx 30$ AU and $e < 0.1$.

Table 4. Orbital Constraints from Monte Carlo Simulations

Parameter	Range
P	$120 - 481$ yr
T_0	$1933 - 2067$
e	$0.00 - 0.61$
a	$2\farcs57 - 6\farcs47$
	$27.8 - 69.8$ AU
i	$114\fdg7 - 122\fdg6$
Ω	$63\fdg7 - 76\fdg1$
ω	$0° - 358°$

Note. The upper range of periods and semimajor axes result from the simulation input $P_{max} = 500$ yr, but these orbits require high eccentricities $e > 0.5$ and are thus less likely.

Thus, one of the science goals of the *HST* observing program was to search for evidence of planetesimals in this system, via atmospheric metal pollution in the white dwarf. As discussed in §2.2, calcium absorption was not detected in the STIS data, and a strict upper limit of $\log(\mathrm{Ca/He}) < -11.8$ was derived for GJ 86B. This corresponds to $M_{\mathrm{Ca}} < 3.2 \times 10^{17}$ g in the stellar convection zone, or an upper limit to the total accreted heavy element mass of $M_{\mathrm{Z}} \lesssim 2.0 \times 10^{19}$ g for material that is 1.6% calcium by mass as in the bulk Earth (Allègre et al. 1995). Because the Ca II K line is the most sensitive tracer of metal pollution at optical wavelengths for white dwarfs of this effective temperature (Koester et al. 2005; Zuckerman et al. 2003), this large cometary-sized mass is the strongest possible limit to the observable planetesimal population.

4.4 A Failed Planetary System at Procyon?

Interestingly, and also using STIS, Provencal et al. (2002) found that Procyon B exhibits a strong Mg II resonance line at 2800 Å, a few Fe lines in the near-ultraviolet, and Ca II H and K absorption in the optical. While Procyon is not known to host any planets or planetesimal debris (via precision radial velocity, transits, astrometry, direct imaging, or infrared excess), the white dwarf is externally polluted with at least three heavy elements that could have originated in a minor planetary body (Farihi et al. 2010). Using the published magnesium abundance, Procyon B has accreted at least $M_{\mathrm{Mg}} = 5.1 \times 10^{18}$ g within the past few 10^7 yr, where 2.8 Myr is a single sinking timescale for this element at the stellar effective temperature (Koester 2009). For material with a chondritic or Earth-like elemental abundance, this is equivalent to a total accreted heavy element mass of at least $3 - 6 \times 10^{19}$ g (Lodders & Fegley 1998; Allègre et al.

Table 5. Comparison of GJ 86B & Procyon B

Parameter	GJ 86B	Procyon B[a]
SpT	DQ6.2	DQZ6.5
$T_{\rm eff}$ (K)	8180	7740
Mass ($M_{\odot}$)	0.59	0.60
log (H/He)	< -4.3	< -3.7
log (C/He)	-4.8	-5.5
log (Mg/He)[b]	...	-10.4
log (Ca/He)	< -11.8	-11.8
Primary SpT	K0 V	F5 IV
a (AU)	$\geqslant 28$	15.2
e	...	0.41

[a] Atmospheric parameters from Provencal et al. (2002).
[b] The STIS spectra of GJ 86B do not cover the Mg II 2800 Å resonance lines.

1995), and equivalent to a $25-35$ km diameter object for typical asteroid densities.

Other possible sources for the atmospheric metals are the interstellar medium, or the stellar wind from Procyon A (Provencal et al. 2002). In both of these cases the accreted matter would have solar abundances ($\log({\rm Mg/H}) = -4.45$, $\log({\rm Mg/He}) = -3.35$; Lodders 2003) and imply time-averaged accretion rates of $\dot{M}_{\rm H} = 8.0\times10^{8}\,{\rm g\,s^{-1}}$ and $\dot{M}_{\rm He} = 2.6\times10^{8}\,{\rm g\,s^{-1}}$. If the heavy elements have been continually captured from Procyon A, then hydrogen and helium should have accumulated in the white dwarf atmosphere over its 1.4 Gyr cooling age (Fontaine et al. 2001). During this period 3.6×10^{25} g of hydrogen and 1.1×10^{25} g of helium will have been added to the 2.1×10^{28} g helium convection zone, yielding a current abundance $\log({\rm H/He}) = -2.2$. However, the upper limit derived from the lack of Hα absorption is $\log({\rm H/He}) < -3.7$ and inconsistent with stellar wind accretion.

If one ignores the issue of hydrogen accumulation, the mass loss rate from Procyon A that is necessary to supply the magnesium in the white dwarf at the observed time-averaged rate is $1.8\times10^{-9}\,M_{\odot}\,{\rm yr^{-1}}$ for a Bondi-Hoyle accretion flow (Debes 2006) flow and $9.1\times10^{-8}\,M_{\odot}\,{\rm yr^{-1}}$ for gravitational (Eddington) accretion. These mass-loss rates are between 5 and 7 *orders of magnitude* larger than that measured for the Sun and α Cen (Wood et al. 2001; Withbroe 1989). Therefore, wind capture can be ruled out with confidence. Similar arguments can be used to discount the accretion of interstellar matter. First, hydrogen accumulates whereas metals sink, and thus the hydrogen-deficient atmosphere of Procyon B is at odds with the accretion of solar abundance material for more than 2% of its cooling lifetime. Second, molecular cloud densities are required to account for the observed metals (Farihi et al. 2010), but Procyon has been moving within the local, $r\sim100$ pc, ISM-poor Bubble (Redfield & Linsky 2008) for at least 2.6 Myr.

The remaining possibility is the accretion of one or more planetesimals. Accounting for both the current and former binary configurations, stable orbital regions at Procyon can be either circumbinary beyond 55.4 AU or circumprimary within 2.3 AU (Holman & Wiegert 1999), although bodies in the latter region would be dynamically unlikely to be perturbed towards the surface of the white dwarf. There is no circumstellar region at Procyon B that remains stable over the lifetime of the binary. Thus, a circumbinary population of planetesimals is the most likely source of the metals observed in Procyon B. Observations with *Herschel* PACS at 160 μm have not detected a far-infrared excess at Procyon, and limit the fractional dust luminosity to $L/L_{*} < 5\times10^{-7}$ over the $30-300$ AU region (G. Kennedy 2012, private communication). This limit is only a few times greater than the fractional dust luminosity of the Kuiper belt (Booth et al. 2009; Stern 1996), and for similar particles would result in an upper dust mass limit of roughly an Earth mass for Procyon.

On the main sequence, Procyon should have had a semimajor axis near 9 AU. Even for $e = 0.1$ this implies that disk material available for planet building would be confined to within 2.0 AU of Procyon A and 2.4 AU of Procyon B, and thus completely within their respective snow lines. Thus, giant planet formation at either component of the Procyon system is likely precluded, and likely also for the $a > 55$ AU stable circumbinary environment. Only the inner regions of Procyon A appear capable of forming small, solid planets (as in α Cen AB; Dumusque et al. 2012), that persist to the present day, assuming the binary eccentricity was not larger when both stars were on the main sequence. Thus, the Procyon system may represent a case of failed or truncated planet formation, where large planetesimals were formed but further growth was prohibited.

5 SUMMARY & OUTLOOK

High-contrast optical imaging and low-resolution spectroscopy with *HST* have unambiguously characterized the stellar companion to the planet-host star GJ 86A. The secondary is a relatively cool white dwarf with a helium-dominated atmosphere and molecular absorption bands due to trace carbon, which is almost certainly dredged from the core. Neither Hα nor Ca II K are detected in deeper, medium-resolution spectroscopy, the latter placing modest limits on the presence of scattered planetesimal material.

The binary separation of GJ 86 has continued to increase since last observed in 2005, and the actual orbit deviates from prior estimates. While one-quarter orbit has not yet been observed, Monte Carlo simulations constrain the semimajor axis to $a \geqslant 27.8$ AU, and the system inclination within $114\overset{\circ}{.}7 \leqslant i \leqslant 122\overset{\circ}{.}6$. For planetary-binary coplanar orbits, these results imply the mass of GJ 86Ab lies between 4.4 and 4.7 $M_{\rm Jup}$.

Future imaging is necessary to observe apastron and dynamically constrain the component masses. This can be done with adaptive optics in the near-infrared, but superior data will come from follow up imaging and spectroscopy with *HST* in the near-ultraviolet. In this relatively low-contrast wavelength regime, there will be narrow absorption lines from C I, and possibly Mg II which is a strong absorption feature in Procyon B. Such spectral lines can provide a baseline radial velocity and gravitational redshift for the secondary; these would more efficiently characterize the current and former binary configurations than near-infrared data.

ACKNOWLEDGMENTS

The authors thank an anonymous referee for a timely and thorough report. J. Farihi thanks J. Provencal for helpful feedback on the available spectra of Procyon B, as well as G. Kennedy and M. Wyatt for a useful summary of the infrared excess and dust limits in this system. This work is based on observations made with the *Hubble Space Telescope* which is operated by the Association of Universities for Research in Astronomy under NASA contract NAS 5-26555. These observations are associated with program 12548. Support for Program number 102548 was provided by NASA through grant HST-GO-12548 from the Space Telescope Science Institute. J. Farihi gratefully acknowledges the support of the STFC via an Ernest Rutherford Fellowship and as a PDRA. N. Haghighipour acknowledges support from NASA grants EXOB NNX09AN05G and HST-GO-12548.06-A. J. Holberg acknowledges support from NSF Grant AST-1008845. M. Barstow and M. Burleigh acknowledge support from the STFC.

REFERENCES

Akeson R. L., Koerner D. W., Jensen E. L. N. 1998, ApJ, 505, 358
Allègre C. J., Poirier J. P., Humler E., Hofmann A.W. 1995, Earth Planetary Sci. Letters, 4, 515
Artymowicz P., Lubow S. H. 1994, ApJ, 421, 651
Booth M., Wyatt M. C., Morbidelli A., Moro-Martín A., Levison H. 2009, MNRAS, 399, 385
Correia A. C. M., et al. 2008, A&A, 479, 271
Debes J. H. 2006, ApJ, 652, 636
Debes J. H., Kilic M., Faedi, F., Shkolnik E. L., Lopez-Morales M., Weinberger A. J., Slesnick C., West R. G. 2012, ApJ, 754, 59
Desidera S., Barbieri M. 2007, A&A, 462, 345
Dressel L., et al. 2010, Wide Field Camera 3 Instrument Handbook, Version 3.0, (Baltimore: STScI)
Dufour P., Bergeron P., Fontaine G. 2005, ApJ, 627, 404
Dumusque X., et al. 2012, Nature, 491, 207
Els S. G., Sterzik M. F., Marchis, F., Pantin E., Endl M., Kürster M. 2001, A&A, 370, L1
Farihi J., Barstow M. A., Redfield S., Dufour P., Hambly N. C. 2010, MNRAS, 404, 2123
Farihi J., Gänsicke B. T., Steele P. R., Girven J., Burleigh M. R., Breedt E., Koester D. 2012, MNRAS, 421, 1635
Flynn C., Morell O. 1997, MNRAS, 286, 617
Fontaine G., Brassard P., Bergeron P. 2001, PASP, 113, 409
Gänsicke B. T., Koester D., Farihi J., Girven J., Parsons S. G., Breedt E. 2012, MNRAS, 424, 333
Ghezzi L., Cunha K., Smith V. V., de Araújo F. X., Schuler S. C., de la Reza R. 2010, ApJ, 720, 1290
Haghighipour N. 2006, ApJ, 644, 543
Hatzes A. P., Cochran W. D., Endl M., McArthur B., Paulson D. B., Walker G. A. H., Campbell B., Yang S. 2003, ApJ, 599, 1383
Hayashi C. 1981, Prog. Theor. Phys. Suppl., 70, 35
Holberg J. B., Sion E. M., Oswalt T., McCook G. P., Foran S., Subasavage J. P. 2008, AJ, 135, 1225
Holman M. J., Wiegert P. A. 1999, AJ, 117, 621
Jeans J. H. 1924, MNRAS, 85, 2
Jura M. 2003, ApJ, 584, L91
Kalirai J. S., Hansen B. M. S., Kelson D. D., Reitzel D. B., Rich R. M., Richer H. B. 2008, ApJ, 676, 594
Kilic M. Patterson A. J., Barber S., Leggett S. K., Dufour P. 2012, MNRAS, 419, L59
Koester D. 2009, A&A, 498, 517
Koester D., Rollenhagen K., Napiwotzki R., Voss B., Christlieb N., Homeier D., Reimers D. 2005a, A&A, 432, 1025
Koester D., Weidemann V., Zeidler E. M. 1982, A&A, 116, 147
Lagrange A. M., Beust H., Udry S., Chauvin G., Mayor M. 2006, A&A, 459, 955
Lodders K. 2003, ApJ, 591, 1220
Lodders K., Fegley B. 1998, The Planetary Scientist's Companion (New York: Oxford University Press)
Mamajek E. E., Hillenbrand L. A. 2008, ApJ, 687, 1264
Mathieu R. D. 1994, ARA&A, 32, 465
McCook G. P., Sion E. M. 1999, ApJS, 121, 1
Mugrauer M., Neuhäuser R. 2005, MNRAS, 361, L15
Mustill A. J., Villaver E. 2012, ApJ, 761, 121
Muterspaugh M. W., et al. 2010, AJ, 140, 1657
Nelson A. F. 2000, ApJ, 537, L65
Pelletier C., Fontaine G., Wesemael, F., Michaud G., Wegner G. 1986, ApJ, 307, 242
Perryman M. A. C., et al. 1997, A&A, 323, L49
Prato L., Weinberger A. J. 2010, Planets in Binary Star Systems, ed. N. Haghighipour, Springer, New York, 1
Provencal J. L., Shipman H. L., Koester D., Wesemael, F., Bergeron P. 2002, ApJ, 568, 324
Queloz D., et al. 2000, A&A, 354, 99
Rabl G., Dvorak, R. 1988, A&A, 191, 385
Raghavan D., Henry T. J., Mason B. D., Subasavage J. P., Jao W. C., Beaulieu T. D., Hambly N. C. 2006, ApJ, 646, 523
Redfield S., Linsky J. L. 2008, ApJ, 673, 283
Ribas I., Solano E., Masana E., Giménez A. 2003, A&A, 411, L501
Rodriguez L. F., et al. 1998, Nature, 395, 355
Saffe C., Gómez M., Chavero C. 2005, A&A, 443, 609
Stern S. A. 1996, A&A, 310, 999
Valenti J. A., Fischer D. A. 2005, ApJS, 159, 141
van Belle G. T., von Braun K. 2009, ApJ, 694, 1085
van Leeuwen F. 2007, A&A, 474, 653
Veras D., Tout C. A. 2012, MNRAS, 422, 1648
Veras D., Wyatt M. C., Mustill A. J., Bonsor A., Eldridge J. J. 2011, MNRAS, 417, 2104
Weidenschilling S. J. 1977, ApSS 51, 153
Williams K. A., Bolte M., Koester D. 2009, ApJ, 693, 355
Withbroe G. L. 1989, ApJ, 337, L49
Wood B. E., Linsky J. L., Müller H. R., Zank G. P. 2001, ApJ, 547, L49
Zucker S., Mazeh T., Santos N. C., Udry S., Mayor M. 2004, A&A, 426, 695
Zuckerman B. Koester D., Reid I. N., Hünsch M. 2003, ApJ, 596, 477